Composites Science and Technology 76 (2013) 77–83

Contents lists available at SciVerse ScienceDirect

Composites Science and Technology

journal homepage: www.elsevier.com/locate/compscitech

Silica nanoparticles as coupling agents for polypropylene/glass composites

Diego Pedrazzoli, Alessandro Pegoretti *

University of Trento, Department of Industrial Engineering and INSTM Research Unit, Via Mesiano 77, 38123 Trento, Italy

ARTICLE INFO

Article history:
Received 15 September 2012
Received in revised form 21 December 2012
Accepted 28 December 2012
Available online 11 January 2013

Keywords:
A. Polymer–matrix composites (PMCs)
B. Interfacial strength
B. Fibre/matrix bond
C. Stress transfer
Single-fibre fragmentation test (SFFT)

ABSTRACT

An evaluation of the fibre/matrix interfacial shear strength was performed by the single-fibre fragmentation tests on polypropylene–glass fibre microcomposites filled with various types and amounts of silica nanoparticles. In particular, both non-functionalized and dimethyldichlorosilane-functionalized silica nanoparticles were added up to a weight content of 7%. Moreover, the effect of various amounts of maleic anhydride modified polypropylene (PPgMA) on the fibre/matrix adhesion was also investigated, including some selected formulations containing both PPgMA and silica nanoparticles.

Interfacial shear strength was found to remarkably increase (up to a factor of about 5 for a 7 wt% content of surface treated nanoparticles) with respect to the case of neat polypropylene matrix. The observed effect was explained by considering that silica nanoparticles increase the work of adhesion of polypropylene with respect to glass, as proven by contact angle measurements in different liquids.

In addition, silica nanoparticles promoted a remarkable enhancement of both elastic modulus and creep stability of the selected polypropylene matrix.

1. Introduction

It has been widely recognized that the fibre/matrix interfacial shear strength controls several mechanical properties of composite materials, in particular the off-axis parameters [1]. At the same time, the interphase region often manifests properties markedly deviating from those of the surrounding bulk matrix [2].

Among thermoplastic resins, polypropylene (PP) is one of the most widely used matrices for the production of glass fibre (GF) reinforced composites [3]. Due to the non-polar nature of the matrix, interfacial adhesion is a critical issue for PP/GF composites [4]. Several authors evaluated the fibre/matrix interfacial shear strength (ISS) for PP/GF microcomposites by microdebonding [5–10] or fragmentation [11–16] tests. From the analysis of the extended literature data, it emerges that for uncoupled PP/GF composites an average ISS value of 4.0 ± 1.4 MPa can be estimated. This value has been also recently confirmed by Yang and Thomason [17] on the basis of a careful experimental work involving both fibre pull-out and microbond methods.

Over the years, two main strategies have been proposed to improve the fibre/matrix adhesion in PP/glass composites: (i) the development of specific fibre sizings/coatings [5,7–10,16,18,19] and/or (ii) the addition of coupling agents to the PP matrix [7,8]. Both strategies lead to interesting results in terms of improvement of the fibre/matrix adhesion level. For example, Thomason and Schoolenberg [9] observed that the use of silane coupling agents have little effect on the level of PP/GF interfacial shear strength. At the same time, they experimentally observed that full commercial coating formulation applied to glass fibres is very important for the interface strength: variations of one order of magnitude in PP/GF adhesion were observed depending on the nature of the glass fibre coating. As reported by Etcheverry et al. [12,16] a chemical anchoring of the matrix polymer on glass fibres was also attempted by direct metallocenic polymerization of PP onto the GF surface. Depending on the hydroxy-α-olefin concentration, the surface treatment induced an increase of the ISS with respect of the untreated fibres by a factor ranging from 1.7 up to 2.1 [16].

On the other hand, Mäder and Freitag [7] evidenced how the bond strength in the PP/GF system can be remarkably enhanced by modifications of the PP matrix, such as the addition of polypropylene grafted with acrylic acid or irradiation with electron beams.

More recently, some indications emerged on the fact that nanoparticles homogeneously dispersed in a polymer matrix [20–22] or localized at the interfacial region [23–25] could play a beneficial role on the fibre/matrix interfacial adhesion in several types of structural composites. Moreover, with the addition of nanoparticles a simultaneous enhancement of the mechanical properties of the polymer matrix can be reached [20] or specific functionalities can be added [26].

The purpose of this study is to investigate the possibility to improve the interfacial adhesion between E-glass fibres and polypropylene by dispersing various types and amounts of silica nanoparticles in the polymer matrix.

* Corresponding author. Tel.: +39 0461 282452; fax: +39 0461 281977.
E-mail address: alessandro.pegoretti@unitn.it (A. Pegoretti).

0266-3538/$ - see front matter © 2013 Elsevier Ltd. All rights reserved.
http://dx.doi.org/10.1016/j.compscitech.2012.12.016

2. Experimental section

2.1. Materials and samples preparation

The matrix of the microcomposites used in this work was an isotactic homopolymer polypropylene (MFI at 190 °C and 2.16 kg = 6.9 g/10', density = 0.904 g cm^{-3}) produced by Polychim Industrie S.A.S. (LOON-PLAGE, France) and provided by Lati Industria Termoplastici S.p.A (Varese, Italy) with the commercial code PPH-B-10-FB. FUSABOND® P M-613-05 maleic anhydride modified polypropylene (PPgMA) (MFI at 190 °C and 2.16 kg = 106.8 g/10', density = 0.903 g cm^{-3}, maleic anhydride content = 0.35–0.70 wt%), was supplied by DuPont™ de Nemours (Geneva, Switzerland).

Both untreated and surface treated fumed silica nanoparticles were supplied by Evonik Industries AG (Hanau, Germany). Untreated nanoparticles (Aerosil® A380) had an average primary particle size of 7 nm and a specific surface area of 321 ± 3 m^2/g, as determined by BET analysis [27]. Dimethyldichlorosilane functionalized silica nanoparticles (Aerosil® R974) were characterized by an average primary particle size of 12 nm and a BET specific surface area of 124 ± 1 m^2/g. Silica nanoparticles were dried for 24 h at 100 °C before to be used for nanocomposite production. E-glass fibres designed as RO99 P319, were supplied by Saint-GobainVetrotex (Chambèry Cedex, France) and were used as-received. These GF are indicated as treated with a silane based coupling agent specifically designed for polypropylene matrices.

Binary nanocomposites containing 1, 3, 5 and 7 wt% of both untreated and surface treated silica nanoparticles were prepared by melt mixing in a Thermo Haake internal mixer (temperature = 190 °C, rotor speed = 50 rpm, time = 10 min) followed by compression moulding in a Carver hot press (temperature = 190 °C, pressure = 0.76 MPa, time = 10 min), in order to get plane square sheets with a thickness of around 0.7 mm. Under the same processing conditions, ternary nanocomposites were also prepared by adding PPgMA as a compatibilizer in three different amounts (1, 3 and 5 wt%) to the systems containing 1, 3 and 5 wt% of silica. Thin (70–80 μm) matrix films required for the preparation of the microcomposites for the fragmentation test were obtained by a further hot pressing stage (temperature = 200 °C, pressure = 3.4 MPa, time = 10 min).

Unfilled matrix was denoted as PP, while nanocomposites were designated indicating the matrix, the compatibilizer (if any) with its content, the kind of filler and its amount. For instance, a sample filled with 5 wt% of PPgMA and 5 wt% of Aerosil® A380 was indicated as PP-PPgMA-5-A380-5.

2.2. Experimental techniques

2.2.1. Fibre strength and elastic modulus evaluation

Tensile tests on single GFs were carried out according to ASTM C 1557-03 standard. Single fibres of three different gauge lengths (5, 15 and 30 mm) were fixed on paper tab frames and tested with an Instron (Norwood, USA) model 4502 tensile machine equipped with a 2.5 N load cell, at a strain rate of 0.2 min^{-1}. Prior testing, fibre diameter was measured on three locations on each specimens by an optical microscope (Leitz Ortholux II POL-BK) through a video-camera (PIKE F032C).

2.2.2. Single fibre fragmentation tests (SFFTs)

Microcomposite were prepared according to a procedure well assessed for thermoplastic matrices [16,28,29]. About 10 fibres were aligned between two thin polymer films, sandwiched between two Mylar® foils and two aluminium plates. This assembly was placed in a vacuum oven at a temperature of 165 °C under a pressure of 10 kPa for 20 min and then cooled in air. The specimens were obtained by cutting strips ($0.18 \times 5 \times 25$ mm^3) containing one single fibre longitudinally aligned in the centre line.

Fragmentation tests were performed at room temperature by a tensile tester (Minimat, by Polymer Laboratories, Loughborough, UK) located under a polarized optical stereo-microscope (Wild M3Z by Leica). At least five specimens for each sample were tested at a strain rate of 0.05 mm^{-1} up to a strain of 10%, necessary to assure the saturation of the fragmentation process. The mean fibre length, L_s, was evaluated by an image analysis software (Image J). The fibre critical length, L_c, was taken as $4/3L_s$ [2]. Interfacial shear strength (ISS) values were derived according to the simplified micromechanical models proposed by Kelly–Tyson [30] and by Cox [31].

According to the Kelly–Tyson approach an average value of ISS is the result of the static equilibrium between the tensile force acting on a fibre and the shear force transferred through the fibre–matrix interface:

$$\mathrm{ISS} = \frac{\sigma_{fb(Lc)} d}{2L_c} \tag{1}$$

where d is the fibre diameter and $\sigma_{fb(Lc)}$ is the tensile strength of a fibre with a critical length L_c, which was computed on the basis of Eq. (2).

$$\sigma_{fb(Lc)} = \sigma_0 \left(\frac{L}{L_0}\right)^{-1/m} \Gamma\left(1 + \frac{1}{m}\right) \tag{2}$$

where Γ is the Gamma function, while σ_0 and m are the scale and shape parameters of the Weibull distribution, respectively, which were estimated from strength data determined at one single gauge length by fitting the distribution of failure probability.

On the other hand, the traditional shear-lag model assumes a number of hypotheses, such as: perfectly elastic and isotropic matrix and fibre properties, proportionality between interfacial shear force and the difference between the displacement in the matrix and the displacement that would exist if the fibre were absent, perfect bonding between matrix and fibre, same lateral stiffness of fibre and matrix, no residual stresses furthermore, the stress is taken as uniform through a radial section of fibre, and the stress is entirely transferred from matrix to fibre by shear at the interface. The axial stress σ_f in the fibre can thus be writtens as:

$$\sigma_f = E_f \varepsilon_f \left(1 - \frac{\cosh(\beta z)}{\cosh(\beta t)}\right) \tag{3}$$

where ε_f is the far-field applied strain, E_f is the elastic modulus of the fibre, z is the axial coordinate, t is the fibre half-length, while β shear-lag parameter is defined as:

$$\beta = \left[\frac{H}{\pi R_f^2 E_f}\right]^{1/2} \tag{4}$$

with

$$H = \frac{\pi E_m}{(1 + \nu_m)\ln(R_m/R_f)} \tag{5}$$

where E_m and ν_m are the matrix elastic modulus and Poisson's ratio, while R_m and R_f are the matrix and fibre radii, respectively. The interfacial shear stress profile $\tau(z)$ can be calculated as:

$$\tau = \frac{E_f R_f \varepsilon_f \beta}{2} \left(\frac{\sinh(\beta z)}{\sinh(\beta t)}\right) \tag{6}$$

2.2.3. Surfaces energetics and roughness

The wettability of some selected matrix compositions and the glass fibre was measured by contact angle measurements with

two different liquids: water as a polar liquid (milli-Q grade, surface tension $\gamma_1 = 72.8$ mN m^{-1}, polar component of surface tension $\gamma_1^p = 50.7$ mN m^{-1}, dispersive component of surface tension $\gamma_1^d = 22.1$ mN m^{-1}, polarity $X_1^p = \gamma_1^p/\gamma_1 = 0.7$), and ethylene glycol as a non-polar liquid (surface tension $\gamma_2 = 48.0$ mN m^{-1}, polar component of surface tension $\gamma_2^p = 19.0$ mN m^{-1}, dispersive component of surface tension $\gamma_2^d = 29.0$ mN m^{-1}, polarity $X_2^p = \gamma_2^p/\gamma_2 = 0.4$) [32].

The total surface tension (γ^{tot}) can be factorized by considering two additive terms: the dispersive surface tension (γ^d) and the polar surface tension (γ^p).

$$\gamma^{tot} = \gamma^d + \gamma^p \tag{7}$$

The polar component of the surface energy characterizes polar interactions between the surface of polymer and the test liquid (within the context of a contact angle measured by static or dynamic (i.e. Wilhemly) technique). In particular, this component is determined by the presence of polar groups, electric charges and free radicals on the polymer surface. In contrast, the dispersive component represents the dispersive interactions taking place between polymer and test liquid and is determined by surface roughness, unevenness and blanching level of the polymer surface [33].

The estimation of the surface tension components of matrix with various compositions was done on the basis of the equilibrium contact angle measured in both test liquids by a modified Wilhelmy technique, based on the vibration induced equilibrium contact angle (VIECA) method [34] and adopting the geometric mean [32]. Surface tension components of glass fibre were calculated referring to the advancing contact angle measured by Wilhelmy technique and applying the geometric mean.

Knowing the surface tension components of the adherents, the work of adhesion was evaluated using the harmonic mean (W_a^h) equation, applicable to predict interactions between low-energy materials [32]:

$$W_a^h = 4\left(\frac{\gamma_1^d\gamma_2^d}{\gamma_1^d + \gamma_2^d} + \frac{\gamma_1^p\gamma_2^p}{\gamma_1^p + \gamma_2^p}\right) \tag{8}$$

and the geometric mean (W_a^g) equation, more suitable to describe interactions between low-energy and high-energy materials:

$$W_a^g = 2\left(\sqrt{\gamma_1^d\gamma_2^d} + \sqrt{\gamma_1^p\gamma_2^p}\right) \tag{9}$$

where the superscripts d and p refer to the dispersive and polar components, respectively, while subscripts 1 and 2 refer to the two solids in contact (polymer and glass fibre), respectively.

The roughness of the samples was determined by a Wave System rugosimeter (Hommelwerke Waveline GmbH, Villingen-Schwenningen, Germany) scanning a 15 mm line at a speed of 0.50 mm min^{-1}. At least three measurements were performed per each sample on the same specimens previously adopted for the estimation of the contact angle. The ANOVA analysis was carried out on the means of R_a and R_{max} at a significance level of 5%.

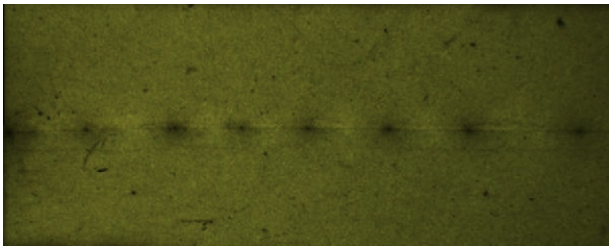

Fig. 1. Representative micrograph of the sample PP-PPgMA-5-A380-5 taken at the end of the saturation process during SFFT ($L_s = 0.93 \pm 0.19$ mm).

2.2.4. Ramp and creep tensile tests on the matrices

Uniaxial ramp tensile tests were performed with an Instron model 4502 (Norwood, USA) tensile tester equipped with a 1 kN load cell, on samples consisting of at least five ISO 527 type 1BA specimens. Tests were carried out at a crosshead speed of 0.25 mm min^{-1} up to a maximum axial deformation of 1%. The strain was recorded by using a resistance extensometer Instron® model 2620-601 with a gauge length of 12.5 mm. The elastic modulus was measured as secant modulus between deformation levels of 0.05% and 0.25% in according to ISO 527 standard. Uniaxial tensile properties at break, such as stress at break (σ_{br}) and strain at break (ε_{br}) were determined at a higher crosshead speed (5 mm min^{-1}) without extensometer.

Creep tests were performed by a dynamic mechanical analyser DMA Q800 (TA Instruments, New Castle, USA) applying a constant stress (σ_0) of 3 MPa for 3600 s at 30 °C. Rectangular strips 25 mm long, 5 mm wide and 0.20 mm thick were tested, adopting a gauge length of 11.5 mm. A creep compliance $D(t)$, computed as the ratio between the strain and the creep stress, was evaluated.

3. Results and discussion

3.1. Interfacial shear strength

In accordance to ASTM standard C 1557-03, the system compliance of the testing configuration on single glass fibre was evaluated by adopting samples of three different gauge lengths. Therefore, an elastic modulus of 63 ± 5 GPa was estimated. For as the tensile strength is concerned, a statistical treatment based on the Weibull distribution was adopted. In particular, following the iterative procedure proposed by Gurvich et al. [35], all experimental data on specimens of different size have been considered together as a statistically representative population. The obtained shape (m) and scale (σ_0) parameters of a two-parameter cumulative Weibull distribution are reported in Table 1, along with the mean values of fibre stress and strain at break. The values of strain at break were corrected to take the compliance of the measuring system into account.

A representative microscopic picture of the sample PP-PPgMA-5-A380-5 at the end of the saturation process during SFFT is

Table 1
Mechanical properties of glass fibre as determined from single fibre tensile tests.

	Gauge length of 5 mm	Gauge length of 15 mm	Gauge length of 30 mm	Entire population
Number of specimens	18	19	19	56
Diameter (μm)	15.5 ± 1.0	15.7 ± 1.7	14.8 ± 1.6	15.3 ± 1.5
Stress at break (MPa)	2720 ± 748	2614 ± 873	2491 ± 835	2606 ± 820
Strain at break (%)	4.6 ± 1.0	3.6 ± 0.8	3.3 ± 0.5	3.8 ± 0.8
Weibull scale parameter, σ_0 (MPa)	3206 ± 31	3710 ± 25	3515 ± 27	3609 ± 19[a]
Weibull shape parameter, m	6.2 ± 0.2	5.8 ± 0.2	4.9 ± 0.2	5.7 ± 0.3
Adjusted R square (R^2)	0.971	0.982	0.978	0.973

[a] Referred to a gauge length $L_0 = 15$ mm.

Table 2
ISS values in according to Kelly–Tyson (ISS_{K-T}) and Cox (ISS_{COX}) models and mechanical parameters (E, σ_{br} and ε_{br}) as measured from tensile tests.

Sample	L_s (mm)	ISS_{K-T} (MPa)	ISS_{COX} (MPa)	G/G_{PP}	E (MPa)	σ_{br} (MPa)	ε_{br} (%)
PP	4.47 ± 0.31	2.7 ± 0.2	3.2 ± 0.6	1.00	1546 ± 24	35.0 ± 0.1	16.8 ± 0.3
PP-PPgMA-5	1.20 ± 0.21	15.2 ± 2.7	8.9 ± 1.5	1.12	1729 ± 31	34.5 ± 0.6	13.3 ± 0.7
PP-PPgMA-10	0.97 ± 0.36	20.2 ± 2.5	13.9 ± 1.1	1.07	1648 ± 12	33.6 ± 0.5	12.1 ± 0.6
PP-A380-5	1.70 ± 0.30	8.4 ± 0.7	6.5 ± 1.0	1.10	1698 ± 32	35.5 ± 0.4	9.0 ± 0.4
PP-R974-1	2.03 ± 0.28	7.6 ± 1.0	4.8 ± 1.0	1.05	1623 ± 57	32.9 ± 0.7	16.7 ± 0.4
PP-R974-3	1.80 ± 0.32	10.9 ± 0.9	7.2 ± 1.2	1.15	1786 ± 57	34.0 ± 0.4	12.9 ± 0.7
PP-R974-5	1.34 ± 0.23	13.1 ± 0.8	8.4 ± 1.5	1.21	1865 ± 24	33.6 ± 0.5	10.2 ± 0.7
PP-R974-7	1.29 ± 0.25	13.9 ± 0.5	9.5 ± 1.8	1.23	1895 ± 23	33.0 ± 0.7	10.1 ± 0.7
PP-PPgMA-5-A380-5	0.93 ± 0.19	22.7 ± 2.1	15.2 ± 2.2	1.30	2015 ± 40	34.2 ± 0.3	6.7 ± 0.2
PP-PPgMA-5-R974-5	0.58 ± 0.05	38.8 ± 3.5	25.6 ± 2.4	1.47	2281 ± 58	31.3 ± 0.9	12.0 ± 1.1

L_s: mean fragment length at saturation. ISS_{K-T}: ISS values in according to Kelly–Tyson approach. ISS_{COX}: ISS values in according to Cox model. G/G_{PP}: shear modulus normalized with respect to that of PP. E: tensile modulus. σ_{br}: tensile strength at break. ε_{br}: elongation at break.

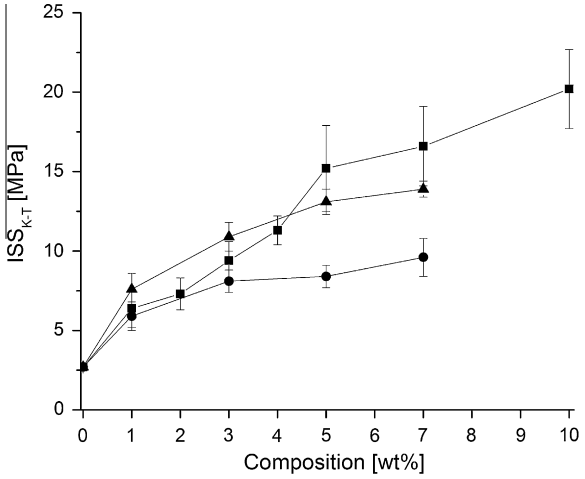

Fig. 2. ISS values computed according to the Kelly–Tyson model as a function of the content of (■) PP-PPgMA, (●) PP-A380, and (▲) PP-R974.

represented in Fig. 1. Unfortunately, it was generally quite difficult to obtain a good resolution in the colour micrographs and appreciably distinguish the photoelastic patterns at the interface and understand the dominant failure mechanisms [36].

The average saturation length of the fibre fragments as measured by the SFFT is reported in Table 2 for some selected samples, along with the ISS values estimated according to the Kelly–Tyson (ISS_{K-T}) or the Cox (ISS_{COX}) models. It is clear that the addition of PPgMA, silica nanoparticles or a combination of both additives induces a sharp decrease of the saturation length and, consequently, an enhancement of the ISS values.

In particular, ISS values obtained on the basis of the Kelly–Tyson model are plotted in Fig. 2 as a function of the percentage of PPgMA or silica nanoparticles for all the investigated samples. As expected, when the PPgMA compatibilizer is added, ISS values considerably increase with respect to the case of neat PP/GF sample. It is interesting to note that comparable improvements can be reached by the addition of silica nanoparticles. In fact, if compared to PP-PPgMA systems, PP-silica nanocomposites show similar improvement of ISS values up to a 4–5 wt% content, while for higher percentages PPgMA seems to be more effective than nanoparticles. In Fig. 3, the effect on the ISS values of adding both PPgMA and silica nanoparticles (ternary composites) is evaluated. It is worthwhile to observe that for any given PPgMA content the addition of silica nanoparticles further enhances the ISS values. This positive effect is particularly strong when surface treated silica nanoparticles (R974) are considered. In fact, the sample PP-PPgMA-10 shows a ISS value similar to the composite PP-PPgMA-5-A380-5

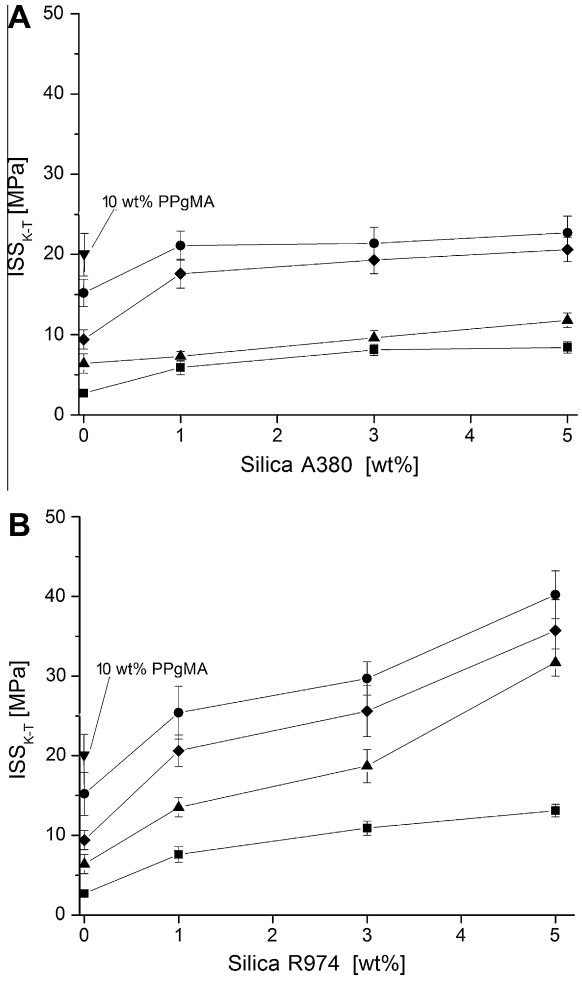

Fig. 3. ISS values computed according to the Kelly–Tyson model as a function of the content of (A) silica A380 and (B) silica R974, and various PPgMA amounts: (■) 0 wt% PPgMA, (▲) 1 wt% PPgMA, (♦) 3 wt% PPgMA and (●) 5 wt% PPgMA.

(see Fig. 3A), but remarkably lower than that of PP-PPgMA-5-R974-5 (see Fig. 3B).

Noteworthy, the ISS values exhibited by the two ternary composites are higher than the bulk matrix shear strength ($\sigma_{y,s}$), which can be assumed to be approximately 22 MPa, according to a Von Mises yield criterion considering a measured tensile yield strength ($\sigma_{y,t}$) of 37 MPa for PP. This difference is not completely clear yet.

Some hypotheses can be made, such as the existence of an interphase surrounding the fibre with thermo-mechanical properties higher than that of the bulk matrix [37,38]. In particular, Gao et al. found a value of interfacial shear strength of 30 MPa in

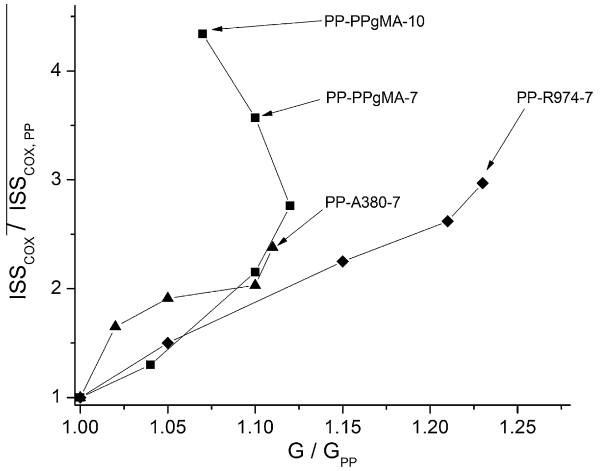

Fig. 4. Relative ISS values computed according to the Cox model as a function of relative shear modulus of the matrix. The normalization has been made over the properties of neat PP.

single-walled carbon nanotubes (SWCNTs)/E glass fibre-PP systems by using a microdebonding test [24].

Moreover, ISS values calculated adopting the Cox model (ISS_{COX}) are generally lower than those computed with the Kelly–Tyson model (ISS_{K-T}) with values below the matrix shear strength ($\sigma_{y,s}$) except for the sample PP-PPgMA-5-R974-5. This fact could indicate that an elastic–perfectly plastic analysis could be misleading in the present situation.

Furthermore, as Prof. Piggot pointed out some years ago, several micro-mechanical tests, including the fragmentation tests, might produce values of the fibre/polymer interfacial shear strength as much as 10 times higher than the polymer shear strength [39]. To explain this fact, he hypothesized that failure in the polymer matrix does not occur under shear conditions, but a tensile failure is more likely to occur at 45° to the shear axes. Therefore, the conclusion of Piggot was that the reported shear strength values most probably refer to a tensile failure and should be consequently compared with the tensile strength of the polymer matrix or the interfacial region.

The ISS values have been also estimated in accordance to Cox model by assuming a concentric cylindrical geometry. The matrix Poisson's ratio, necessary for the implementation of Cox model, was measured on unfilled PP ($\nu_m = 0.458 \pm 0.015$) by using two extensometers (axial and transversal) mounted on ISO527 1B specimens produced by injection moulding. Relative ISS_{COX} values, i.e. normalized over the value obtained for neat PP, are plotted in Fig. 4 as a function of the relative shear modulus of the matrix. It is interesting to observe that ISS_{COX} exhibits a significative increase with the matrix stiffness for all samples. Therefore, according to the Cox shear lag model, the observed increase in the stress transfer ability of the interface could be explained on the basis of the matrix stiffening effect caused by the additives (both PPgMA and silica nanoparticles). However, a marked discrepancy from the expected trend can be observed for ternary composites. Noteworthy, the samples PP-PPgMA show values of ISS progressively increasing with the PPgMA content even though the mechanical reinforcement of the samples with filler content higher than 5 wt% is decreasing. The values of ISS evaluated by applying Cox model need to be interpreted in according to the model hypotheses and the specific operative test conditions. Both the fibre and the matrix are considered as linear elastic bodies, but the actual fragmentation process occurring in model composite samples generally involves plastic deformation regions, thus leading to a significative underestimation of the interfacial toughness. In addition, Cox model is based on the assumption of perfect bonding between matrix and fibre, thus the chemical nature of surfaces and the surface quality are not taken into account.

3.2. Surfaces energetics and roughness

Both the matrix and fibre surface tensions were calculated from measured equilibrium contact angles and from those values the thermodynamic work of adhesion (W_a) was computed in according to the harmonic (Eq. (8)) and geometric (Eq. (9)) mean equations. The polar component of the matrix surface tension (γ_p) increased considerably due to the addition of PPgMA, probably due to the presence of hydrophilic maleic anhydride groups [40]. PP-A380 systems show a similar increase in γ_p, likely because silica particles are hydrophilic materials. Less clear is the reason why also for PP-R974 composites an increase of the polar component of the matrix surface tension can be observed, even if of lower intensity. The dispersive component (γ_d) is only slightly higher for all nanocomposites with respect to unfilled PP, in particular for PP-PPgMA-5-R974-5 ternary composites.

As expected, values of work of adhesion (W_a) calculated using the geometric mean equation are higher than those calculated from the harmonic mean equation [32]. The quantity W_a represents the adhesion energy between solid phases, the higher the work of adhesion, the better the interfacial bonding between fibre and matrix. W_a values of PP-PPgMA blends and PP-silica nanocomposites are much greater than that of unfilled PP (Table 3). However, as already stated by Wojuzkij [41] a direct correlation between work of adhesion and the adhesion parameters measured through mechanical tests is not the rule. In fact, micromechanical tests such as the SFFT are characterized by non-equilibrium phenomena (such as the specific viscoelastic properties and the

Table 3
Surface tension components estimated from the measured equilibrium contact angles and thermodynamic work of adhesion.

Sample	γ^p (mN m^{-1})	γ^d (mN m^{-1})	γ (mN m^{-1})	W_a^h (mN m^{-1})	W_a^g (mN m^{-1})	ISS_{K-T} (MPa)
PP	0.1 ± 0.0 (0.003)	30.1 ± 0.4	30.2 ± 0.4	53.0	53.9	2.7 ± 0.2
PP-PPgMA -5	2.7 ± 0.2 (0.080)	31.0 ± 0.5	33.7 ± 0.5	57.8	58.4	15.2 ± 2.7
PP-PPgMA -10	2.8 ± 0.2 (0.075)	34.6 ± 0.4	37.4 ± 0.4	60.4	61.5	20.2 ± 2.5
PP-A380-5	2.5 ± 0.3 (0.076)	30.6 ± 0.6	33.1 ± 0.7	57.3	57.8	8.4 ± 0.7
PP-R974-1	1.8 ± 0.1 (0.055)	31.2 ± 0.5	33.0 ± 0.5	57.2	57.8	7.6 ± 1.0
PP-R974-3	2.3 ± 0.2 (0.068)	31.5 ± 0.7	33.8 ± 0.7	57.8	58.4	10.9 ± 0.9
PP-R974-5	2.2 ± 0.1 (0.063)	33.0 ± 0.4	35.1 ± 0.4	58.8	59.6	13.1 ± 0.8
PP-R974-7	2.1 ± 0.2 (0.055)	35.8 ± 0.6	37.9 ± 0.6	60.6	61.9	13.9 ± 0.5
PP-PPgMA-5-A380-5	2.4 ± 0.2 (0.064)	35.2 ± 0.5	37.6 ± 0.5	60.4	61.6	22.7 ± 2.1
PP-PPgMA-5-R974-5	1.6 ± 0.3 (0.036)	42.3 ± 0.7	44.0 ± 0.8	63.7	66.4	40.2 ± 3.0
GF (RO99 P319)	2.0 ± 0.2 (0.079)	23.3 ± 0.5	25.3 ± 0.5	–	–	–

γ^p: polar surface tension component. Values of polarity ($X^p = \gamma\ p/\gamma$) are reported in brackets. γ^d: dispersive surface tension component. $\gamma = \gamma^p + \gamma^d$. W_a^h: work of adhesion calculated using the harmonic mean equation (8). W_a^g: work of adhesion calculated using the geometric mean Eq. (9).

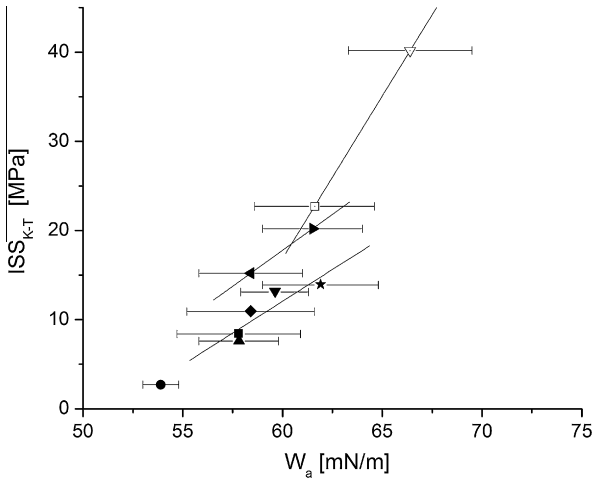

Fig. 5. ISS values estimated in accordance to Kelly–Tyson model, as function of the thermodynamic work of adhesion W_a calculated using the mean equations: (●) PP, (▲) PP-R974-1, (■) PP-A380-5, (♦) PP-R974-3, (▼) PP-R974-5, (★) PP-R974-7, (◄) PP-PPgMA-5, (►) PP-PPgMA-10, (□) PP-PPgMA-5-A380-5, (▽) PP-PPgMA-5-R974-5. Lines represent a linear fitting operated on each group of data.

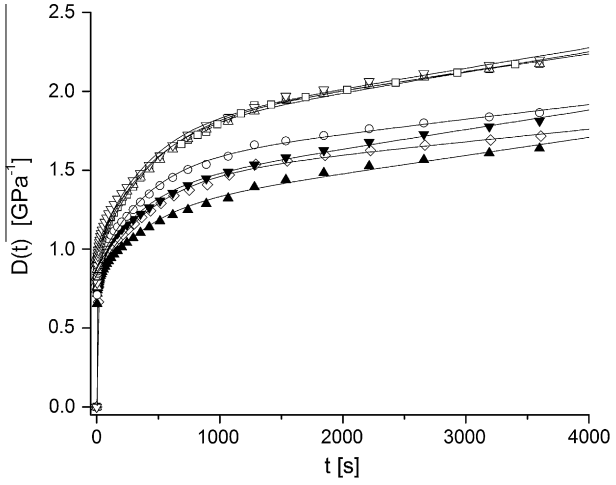

Fig. 6. Creep compliance curves of (□) PP, (△) PP-PPgMA-5, (▽) PP-PPgMA-10, (◇) PP-A380-5, (○) PP-R974-5, (▲) PP-PPgMA-5-A380-5 and (▼) PP-PPgMA-5-R974-5 matrices.

fracture/yield behaviour of the matrix). Nevertheless, in the present case a clear trend with the experimentally measured ISS values can be recognized (Fig. 5). Also for ternary composites a further increment in W_a values can be observed which correlates well with the ISS values. These observation are in good agreement with what previously reported by Ramanathan et al. [42] for an epoxy/carbon system. Moreover, the roughness of the matrix films used in this work resulted in the range of R_a = 0.2–0.4 μm (R_{max} = 2.5–3.6 μm) for all samples. The ANOVA analysis carried out on the mean values of R_a and R_{max} showed no statistically significative differences at a significance level of 5%. Therefore, the contribution of surface roughness to surface properties can be neglected and the differences measured through wettability tests can be mainly attributed to surface chemistry.

3.3. Ramp and creep tensile mechanical behaviour of the matrices

As reported in Table 2, the addition of silica nanoparticles induces a significant increase of the elastic modulus of the PP matrix, which is further incremented by the addition of PPgMA, reaching an overall improvement of 48% for ternary systems, compared to unfilled PP. In general, the stress at break decreases with the addition of the nanofiller for both kinds of silica nanocomposites (Table 2), probably because of the filler aggregation and stronger interaction [43]. For the same reason the elongation at break exhibited in nanocomposite is lower than that of unfilled PP.

Finally, as documented in Fig. 6, the introduction of silica nanoparticles leads to a significant improvement of the creep stability, evidenced as a reduction in the creep compliance. It is generally believed that nanoparticles can effectively restrict the motion of polymer chains, influencing the stress transfer at a nanoscale, with positive effects on the creep stability of the material [44]. On the contrary, PP-PPgMA blends manifest the same creep compliance as neat PP. This latter aspect is surely an advantage offered by the usage of nanoparticles as coupling agents.

4. Conclusions

Interfacial shear strength was investigated by means of the single fibre fragmentation test on various PP/GF microcomposites containing various types and amounts of silica nanoparticles. Results show that the strength at the interface can be remarkably increased by the addition of dimethyldichlorosilane-functionalized silica nanoparticles, and that the improvement is particularly enhanced when the nanoparticles are used in combination with PPgMA in ternary composites. The fibre/matrix work of adhesion showed a good correlation with the ISS values. Finally, nanomodified systems showed improvements of both rigidity and creep stability over neat PP and PP-PPgMA blends.

References

[1] Hull D. Matrix-dominated properties of polymer matrix composite materials. Mater Sci Eng A – Struct Mater Prop Microstruct Process 1994;184(2):173–83.
[2] Kim J-K, Mai Y-M. Engineered interfaces in fibre reinforced composites. Amsterdam (The Netherlands): Elsevier; 1998.
[3] Karger-Kocsis J. Polypropylene: an A–Z reference. Dordrecht (The Netherlands): Kluwer Publishers; 1999.
[4] Mukhopadhyay S, Deopura BL, Alagiruswamy R. Interface behavior in polypropylene composites. J Thermoplast Compos Mater 2003;16(6):479–95.
[5] Feller JF, Grohens Y. Coupling ability of silane grafted poly(propene) at glass fibres/poly(propene) interface. Compos Part A – Appl Sci Manuf 2004;35(1):1–10.
[6] Hoecker F, Karger-Kocsis J. Effects of crystallinity and supermolecular formations on the interfacial shear strength and adhesion in GF PP composites. Polym Bull 1993;31(6):707–14.
[7] Mäder E, Freitag KH. Interface properties and their influence on short fibre composites. Composites 1990;21(5):397–402.
[8] Mäder E, Jacobasch HJ, Grundke K, Gietzelt T. Influence of an optimized interphase on the properties of polypropylene/glass fibre composites. Compos Part A – Appl Sci Manuf 1996;27(9):907–12.
[9] Thomason JL, Schoolenberg GE. An investigation of glass–fibre polypropylene interface strength and its effect on composite properties. Composites 1994;25(3):197–203.
[10] Yue CY, Cheung WL. Interfacial properties of fibre-reinforced composites. J Mater Sci 1992;27(14):3843–55.
[11] Cabral-Fonseca S, Paiva MC, Nunes JP, Bernardo CA. A novel technique for the interfacial characterisation of glass fibre–polypropylene systems. Polym Testing 2003;22(8):907–13.
[12] Etcheverry M, Barbosa SE. Glass fibre reinforced polypropylene mechanical properties enhancement by adhesion improvement. Materials 2012;5(6):1084–113.
[13] Lee NJ, Jang J. The use of a mixed coupling agent system to improve the performance of polypropylene-based composites reinforced with short-glass–fibre mat. Compos Sci Technol 1997;57(12):1559–69.
[14] Nygård P, Redford K, Gustafson CG. Interfacial strength in glass fibre–polypropylene composites: influence of chemical bonding and physical entanglement. Compos Interfaces 2002;9(4):365–88.
[15] Zheng A, Wang HG, Zhu XS, Masuda S. Studies on the interface of glass fibre-reinforced polypropylene composite. Compos Interfaces 2002;9(4):319–33.
[16] Etcheverry M, Ferreira ML, Capiati NJ, Pegoretti A, Barbosa SE. Strengthening of polypropylene–glass fibre interface by direct metallocenic polymerization of propylene onto the fibres. Compos Part A – Appl Sci Manuf 2008;39(12):1915–23.

[17] Yang L, Thomason JL. Interface strength in glass fibre–polypropylene measured using the fibre pull-out and microbond methods. Compos Part A – Appl Sci Manuf 2010;41(9):1077–83.
[18] Nygård P, Redford K, Gustafson C-G. Interfacial strength in glass fibre–polypropylene composites: influence of chemical bonding and physical entanglement. Compos Interfaces 2002;9(4):365–88.
[19] Mäder E, Moos E, Karger-Kocsis J. Role of film formers in glass fibre reinforced polypropylene – new insights and relation to mechanical properties. Compos Part A – Appl Sci Manuf 2001;32(5):631–9.
[20] Dorigato A, Morandi S, Pegoretti A. Effect of nanoclay addition on the fibre/matrix adhesion in epoxy/glass composites. J Compos Mater 2011;46(12):1439–51.
[21] Zhamu A, Zhong WH, Stone JJ. Experimental study on adhesion property of UHMWPE fibre/nano-epoxy by fibre bundle pull-out tests. Compos Sci Technol 2006;66(15):2736–42.
[22] Vlasveld DPN, Parlevliet PP, Bersee HEN, Picken SJ. Fibre–matrix adhesion in glass–fibre reinforced polyamide-6 silicate nanocomposites. Compos Part A – Appl Sci Manuf 2005;36(1):1–11.
[23] Gao X, Jensen RE, McKnight SH, Gillespie JW. Effect of colloidal silica on the strength and energy absorption of glass fibre/epoxy interphases. Compos Part A – Appl Sci Manuf 2011;42(11):1738–47.
[24] Gao SL, Mäder E, Plonka R. Nanocomposite coatings for healing surface defects of glass fibres and improving interfacial adhesion. Compos Sci Technol 2008;68(14):2892–901.
[25] Rausch J, Zhuang RC, Mäder E. Application of nanomaterials in sizings for glass fibre/polypropylene hybrid yarn spinning. Mater Technol 2009;24(1):29–35.
[26] Pedrazzoli D, Dorigato A, Pegoretti A. Monitoring the mechanical behaviour under ramp and creep conditions of electrically conductive polymer composites. Compos Part A – Appl Sci Manuf 2012;43(8):1285–92.
[27] Dorigato A, Pegoretti A, Penati A. Linear low-density polyethylene – silica micro- and nanocomposites: dynamic rheological measurements and modeling. Express Polym Lett 2010;4(2):115–29.
[28] Pegoretti A, Fidanza M, Migliaresi C, DiBenedetto AT. Toughness of the fibre/matrix interface in nylon-6/glass fibre composites. Compos Part A – Appl Sci Manuf 1998;29(3):283–91.
[29] Pegoretti A, Fambri L, Migliaresi C. Interfacial stress transfer in nylon-6/E-glass microcomposites: effect of temperature and strain rate. Polym Comp 2000;21(3):466–75.
[30] Tyson WR, Kelly A. Tensile properties of fibre-reinforced metals: copper/tungsten and copper/molybdenum. J Mech Phys Solids 1965;13(6):329–38.
[31] Cox H. The elasticity and strength of paper and other fibrous materials. Br J Appl Phys 1952;3:72–9.
[32] Wu S. Polymer interface and adhesion. New York: Marcel Dekker, Inc.; 1892.
[33] Fridman A. Plasma Chemistry. New York; 2008.
[34] Della Volpe C, Siboni S. A conveyor belt model for the dynamic contact angle. Eur J Phys 2011;32(4):1019–32.
[35] Gurvich MR, Di Benedetto AT, Pegoretti A. Evaluation of the statistical parameters of a Weibull distribution. J Mater Sci 1997;32:3711–6.
[36] Wu C-M, Chen M, Karger-Kocsis J. Interfacial shear strength and failure modes in sPP/CF and iPP/CF microcomposites by fragmentation. Polymer 2001;42(1):129–35.
[37] Detassis M, Pegoretti A, Migliaresi C. Effect of temperature and strain rate on interfacial shear stress transfer in carbon/epoxy model composites. Compos Sci Technol 1995;53:39–46.
[38] Pegoretti A, Fambri L, Migliaresi C. Interfacial stress transfer in nylon-g/e-glass microcomposites: effect of temperature and strain rate. Polym Compos 2000;21(3):466–75.
[39] Piggott M. Why the fibre/polymer interface can appear to be stronger than the polymer matrix. Compos Sci Technol 1996;57:853–7.
[40] Garbassi F, Morra M, Occhiello E. Polymer surfaces: from physics to technology. New York: John Wiley & Sons Ltd.; 1998.
[41] Wojuzkij SS. Uber das fehlen einer korrelation zwisehen der admision und benetzung yon substraten dureh das polymere adhaisiv. Polymer 1966;214(2):97–100.
[42] Ramanathan T, Bismarck A, Schulz E, Subramanian K. Investigation of the influence of acidic and basic surface groups on carbon fibres on the interfacial shear strength in an epoxy matrix by means of single-fibre pull-out test. Compos Sci Technol 2001;61:599–605.
[43] Dorigato A, D'Amato M, Pegoretti A. Thermo-mechanical properties of high density polyethylene – fumed silica nanocomposites: effect of filler surface area and treatment. J Polym Res 2012;19(6). 9889_9881–9889_9811.
[44] Dorigato A, Pegoretti A, Kolařík J. Nonlinear tensile creep of linear low density polyethylene/fumed silica nanocomposites: time-strain superposition and creep prediction. Polym Compos 2010;31(11):1947–55.